

Adsorption of 7-ethynyl-2,4,9-trithia-tricyclo[3.3.1.1^{3,7}]decane on ultra-thin CdS films

Ivan Dolog^a, Robert R. Mallik^{a,*}, Anthony Mozynski^a, Jun Hu^b, Hui Wang^b

^a Department of Physics, The University of Akron, Akron, OH 44325-4001, USA

^b Department of Chemistry, The University of Akron, Akron, OH 43425-3601, USA

Received 5 January 2006; accepted for publication 9 May 2006

Available online 2 June 2006

Abstract

The adsorption mechanism for the new compound, 7-ethynyl-2,4,9-trithia-tricyclo[3.3.1.1^{3,7}]decane (7ETTD), on ultra-thin films (~3 nm) of CdS is investigated. Multiple reflection absorption IR spectroscopy, in conjunction with inelastic electron tunneling spectroscopy, indicates that this compound forms a self-assembled monolayer adsorbed on the CdS surface via each molecule's trithia-adamantane anchor. Conductance–voltage data are recorded for tunnel junctions of the type Al/CdS/7ETTD/Pb over a temperature range of 4 K to room temperature and they indicate that the presence of the 7ETTD layer on the CdS dramatically modifies the conductance–voltage behavior of the junctions. These measurements show that different conduction mechanisms, including tunneling and possibly hopping, are responsible for charge transfer through the junctions depending on current, temperature, and voltage. WKB fits to the data are used to determine barrier parameters (height and width) for Al/CdS/Pb junctions with and without adsorbed 7ETTD layers on the CdS. Analysis of the fits shows that tunneling occurs at low bias (less than ~0.2 V) but, at higher bias voltages, modification of the barrier parameters alone is insufficient to account for the observed conductance changes. A frontier orbital model is invoked which does offer a plausible explanation for these conductance changes. The model assumes bias-dependent coupling between HOMO and LUMO states of the adsorbed 7ETTD and the surface states on the CdS. The present work suggests that, because of the marked effect on the conductance of CdS ultra-thin films, 7ETTD and other similar compounds may be candidates for use in molecular electronic device fabrication.

© 2006 Elsevier B.V. All rights reserved.

Keywords: Electron spectroscopy; Photovoltaics; Self-assembly; Sputtering; Cadmium sulfide; Tunneling; Amorphous thin films

1. Introduction

Electronic transport in organic semiconductor materials has gained increasing attention over the last thirty years [1]. Organic materials, in association with thin semiconductor films, can be used in a number of applications such as photovoltaic devices, solar cells, field-effect transistors, and other opto-electronic devices. Organic materials offer several advantages over conventional crystalline and amorphous inorganic semiconductor materials such as simplicity of deposition and the ability to tailor the band gap by changing chemical groups in the molecule. Also, substitut-

ing thin flexible films for brittle crystalline or amorphous materials opens up possibilities for low cost and versatile sources of energy conversion. Nevertheless, organic materials currently remain complimentary materials for semiconductor devices rather than competitive primarily due to poor efficiency and low charge mobility.

A great variety of organic molecules have been identified that can be used as self-assembled-monolayers (SAMs). Some of them contain carboxylate groups [2–4] which, because of their polar nature, enhances conditions for self-assembly [5]. Others contain active sites with atoms like sulfur and selenium which may rely on physisorption and a strong affinity to the atoms of the surface for arrangement [6]. One of the promising categories of SAMs is a new family of compounds based on a trithia-adamantane anchor

* Corresponding author. Tel.: +1 330 972 7145; fax: +1 330 971 6918.
E-mail address: rrm@physics.uakron.edu (R.R. Mallik).

developed by Hu [7,8]. In these compounds, three sulfur atoms are conveniently sitting at the end of a tripod which allows the molecules to adsorb on various surfaces including gold.

CdS, along with CdSe and CdTe, are viable semiconductor materials for thin-film photovoltaic devices and have band gaps in the range 1.4–1.5 eV. These materials can be used also for the fabrication of hybrid heterojunctions. The presence of organic layers in heterojunctions tends to improve surface smoothness and the layers can also be used for light conversion [9]. But the problem of the contact resistance between semiconductors layer and metal electrode and trapping levels remains [10,11].

In the present work we present data on the adsorption of the new compound 7-ethynyl-2,4,9-trithia-tricyclo[3.3.1.1^{3,7}]decane (7ETTD) (Fig. 1) on an ultra-thin film of CdS. We will show that the compound adsorbs on the semiconductor surface by orienting in the right arrangement to form a heterojunction and we will investigate the electronic properties of these heterojunctions. Their current–voltage dependences are recorded over a temperature range of 4.2–300 K, and temperature dependent conductance–voltage $G(V, T)$ data derived from those measurements allow us to determine the associated conductance mechanisms in the heterojunctions. Inelastic electron tunneling spectroscopy (IETS) is also used to characterize the electronic properties of the junctions. IETS has been shown to be a useful tool for investigating physical phenomena on surfaces. IETS was discovered around 40 years ago by Jaklevic and Lambe [12], and there have been several extensive reviews of the technique since then. Three of the most informative works on IETS are probably the authoritative book on the subject edited by Hansma [13], a thorough review article by Brown [14] and an up-to-date review article by Hipps and Mazur [15] which incorporates recent developments. The reader is directed to these sources, and references therein, for a full description of the technique. The present workers have used IETS previously to study vibrational spectra of ultra-thin sputtered films of germanium oxide, silicon and its oxides and also CdTe oxides [16–18]. IETS has an advantage over IR and Raman spectroscopy since the signal-to-noise ratio in-

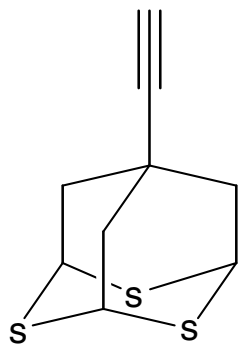


Fig. 1. Structural model of 7-ethynyl-2,4,9-trithia-tricyclo[3.3.1.1^{3,7}]decane (7ETTD).

creases for thinner film, such as those under investigation in the present work. IETS has also been shown to be a convenient technique for investigating tunnel barrier parameters for thin layers of semiconductors [15] and this aspect is extended to the present CdS systems under investigation.

2. Experimental method

2.1. Tunnel junction fabrication

Al/barrier/Pb tunnel junctions were fabricated using standard vacuum deposition techniques. The Al and Pb films were evaporated from resistively heated sources, and CdS barrier layers were formed by RF sputtering as described below.

A stainless steel vacuum chamber with a base pressure 10^{-6} Torr was used for preparation of the tunnel junctions. Prior to each junction fabrication the chamber was cleaned in an oxygen and argon plasma discharge, and the RF sputter gun was cleaned with argon. Next the Al electrodes were evaporated onto a glass substrate. Depending on the required barrier, one or more of the following procedures were adopted:

- The sample was removed from the chamber and spin doped with solvent (dichloromethane or diethylether). This procedure was employed to prepare control samples to ensure that there is no contamination in the chamber or solvent.
- RF sputtering of CdS in a background of argon with chamber pressure ~ 50 mTorr. A 2 in. diameter 0.25 in. thick 99.999% pure CdS sputter target, supplied by Kurt J. Lesker Company, was used. Deposition rates were in the range 0.01–0.02 nm/s. The thickness of CdS films was 3 nm determined by a quartz film thickness monitor.
- First, a CdS film was sputtered as described in (b), then the film was spin doped with (7ETTD) dissolved in dichloromethane and diethylether in the following proportion: 9 mg 7ETTD/2 ml dichloromethane/13 ml diethylether. Such a solution was found to produce more uniform surface coverage of the adsorbate as indicated by corresponding tunnel junction resistance measurements.

To complete the fabrication process, tunnel junctions were capped with an approximately 300 nm thick lead cover-electrode. We used 99.999% pure or better source materials for both Al and Pb. Fig. 2 shows a schematic diagram of the sample.

2.2. I – V and conductance–voltage (G – V) measurements

Four terminal I – V measurements were performed, and the data were recorded using a commercially available data acquisition software package. Conductance–voltage (G – V) data were derived numerically from I – V measurements, by

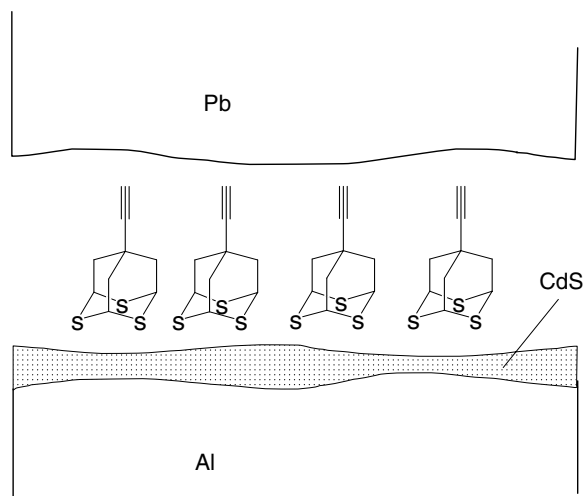


Fig. 2. Schematic cross-section of an Al/CdS/7ETTD/Pb tunnel junction. The Al and Pb films are approximately 100 and 300 nm thick, respectively, and the CdS layer 3 nm. The 7ETTD molecules are approximately 0.6 nm long as determined by Gaussian 98 B3LYP/6-31+g(d,2p) calculations.

taking the derivative of the data, using a finite difference algorithm. Measurements were performed in a cryostat at temperatures in the range 4.2–298 K. The temperature was measured using a Si tunnel diode (CY7 purchased from Omega Technologies Company).

2.3. IETS measurement

The details of our spectrometer are reported elsewhere [19]. Spectra were recorded with samples cooled to 4.2 K in liquid helium. Low bias features associated with the Pb superconducting band gap were recorded and indicate that tunneling is occurring. Normalized tunneling intensity spectra were recorded in constant resolution mode [20] with a modulation voltage of 1 mV. Each spectrum was recorded by averaging signal over 20 scans.

2.4. MRAIRS

MRAIRS data were obtained using a modified attenuated total reflection (ATR) attachment, manufactured by Specac Ltd., housed in a Mattson Cygnus 100 model 7020A FTIR spectrometer. Specifically, the ATR attachment was modified by incorporating a custom built wire frame spacer to vary the separation between two parallel sample mirrors. This spacer allows the beam entry angle, and number of reflections, to be adjusted in order to increase measurement sensitivity. Sample mirrors were made, two at a time, by evaporating Al films onto glass substrates in a procedure similar to the one adopted for the deposition of the Al films for IETS described above. CdS and/or 7ETTD layers were deposited onto the Al films in the same manner as those used for IETS as necessary. Full details of our MRAIRS set up, which allows for monolayer adsorbate sensitivity, are given elsewhere [21].

3. Results and discussion

3.1. Conduction mechanisms

Different conductance mechanisms are possible in MIM structures, these include direct tunneling, Fowler–Nordheim tunneling, hopping, and others. In order to verify which mechanisms predominate at various I , V , and T values, we analyzed the temperature dependence of corresponding conductance–voltage measurements. Fig. 3(a) and (b) show $G(V, T)$ dependences for an Al/CdS/Pb junction and an Al/CdS/Pb junction modified with (7ETTD), respectively. The $G(V, T)$ surface maps of these two junctions are significantly different, indicating that different conduction mechanisms are at play in different regions. (Notice also that Fig. 3(a) exhibits a more significant bias polarity dependent asymmetry as compared to Fig. 3(b). This is believed to be due to modification of the barrier parameters and conduction mechanisms when the 7ETTD layer is introduced and will be discussed further in Section 3.2.) Pb superconducting energy gap structure is present at low bias for both type of junctions, indicating that a tunneling mechanism is present. This low bias structure has been removed from the figures for clarity. It is logical to

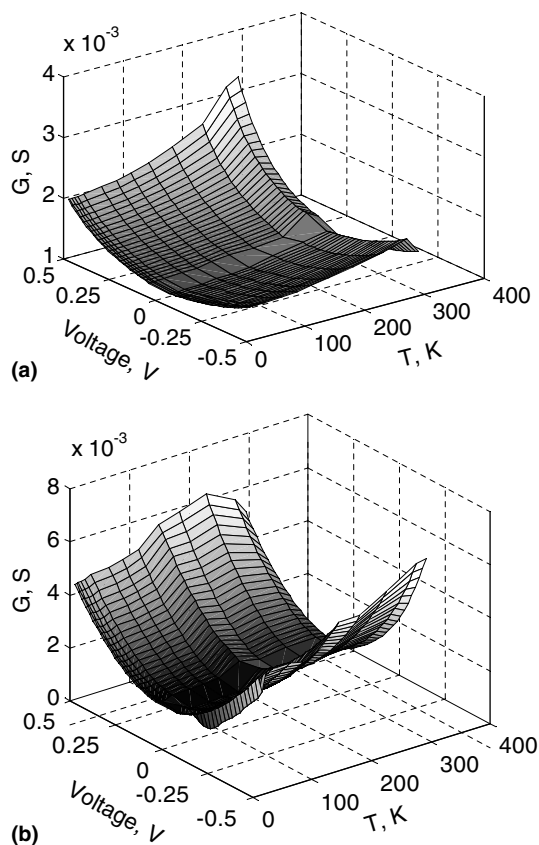


Fig. 3. Temperature dependent conductance–voltage plots for (a) an Al/CdS/solvent/Pb tunnel junction, and (b) an Al/CdS/7ETTD/Pb tunnel junction. Introduction of the 7ETTD layer (b) reduces the degree of bias- and temperature-dependent asymmetry and increases the relative range of normalized conductance.

assume that, at low voltages and temperatures, direct tunneling will be the dominant mechanism. Indeed, for direct tunneling, the current is proportional to voltage as we observe and there is no temperature dependence for either type of junction. Calculations of the barrier parameters will be presented later. For hopping, the current density is given by $J \sim V \exp(-\frac{\phi}{kT})$, where ϕ is the defect activation energy and k is Boltzmann's constant. Fig. 4 shows plots of $\ln G$ versus $1/T$ for a Al/CdS/Pb junction at various bias voltages in the range 0–0.5 V. The slope of the plots at low values of $1/T$ (i.e. sufficiently high temperatures) should approach linear behavior, if hopping conductivity exists, allowing ϕ to be determined from the slope of this linear region. However, we do not observe purely linear behavior so cannot unequivocally determine a value for ϕ . We should point out that we also observe similar $\ln G$ versus $1/T$ behavior for junctions with adsorbed 7ETTD molecules, which indicates that the behavior is not associated with the molecules alone, but rather with the CdS interface.

If the bias voltage approaches the barrier height, ϕ , one would expect to observe Fowler–Nordheim tunneling. However, neither junction displays Fowler–Nordheim conduction. This indicates that for the bias range under investigation (≈ 0 –0.5 V) we do not approach the Fowler–Nordheim region and another conduction mechanism must exist which would explain the difference between the conductance of doped and unmodified junctions at the high end of our bias range (above ~ 0.2 V).

One such mechanism is the transport of electrons through localized channels created by doping. Gaussian 98 B3LYP/6-31+g(d,2p) calculations [22], yield a value of ~ 5.8 eV for the HOMO LUMO gap of the 7ETTD molecule, which is too large to reduce the bandgap of the CdS layer and increase conductance. A frontier orbital model has been proposed to explain band bending and surface charge accumulation on passivated GaAs surfaces [23]. We suggest a similar mechanism may be responsible for the observed behavior of the CdS/7ETTD heterojunctions. Fig. 5(a) shows the traditionally accepted explanation for coupling between HOMO and LUMO levels for two inter-

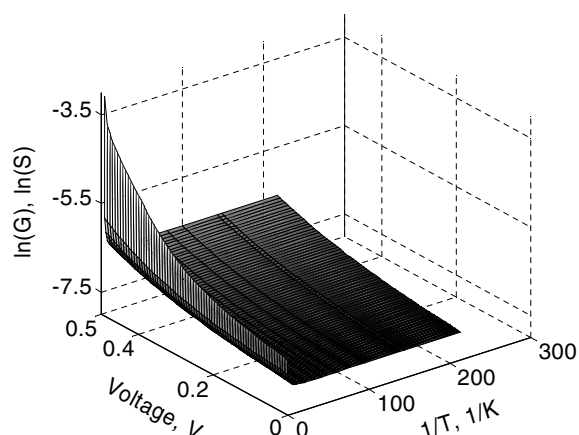


Fig. 4. Bias dependence of $\ln(I/V)$ versus $1/T$ for an Al/CdS/Pb junction.

acting molecules which occurs to minimize the electronic energy of the system, and is included for illustration purposes. Fig. 5(b) schematically represents the frontier orbital model proposed for the explanation of the modification of the surface of a n-type semiconductor and the argument is as follows. The interaction of the LUMO of the adsorbate and the HOMO of the semiconductor (in this case occupied by electrons bound to surface states) forms a new LUMO high above the Fermi level and a new HOMO surface state down in the valence band. The created states behave as new channels that raise the conductance of the junction. Lowering the energy of the surface states causes electrons to be delocalized in the valence band, which reduces the net charge on the interface. Electrons are no longer trapped at the surface, as was the case with an unmodified semiconductor. Reducing the charge of the surface automatically reduces the band bending, which ultimately leads to a reduction of the effective barrier height. For p-type semiconductors the majority carriers are holes, and surface states are now located above the Fermi level near the conduction band. Now surface states play the role of LUMO levels in HOMO–LUMO interactions, since they are empty because of the location above the Fermi level. When the surface is interacting with molecules those states are pushed towards the conduction band edge, which decreases the positive charge traps on the surface. The CdS that we are using is undoped. Since we assume both types of surface states are present in equal amount, both HOMO

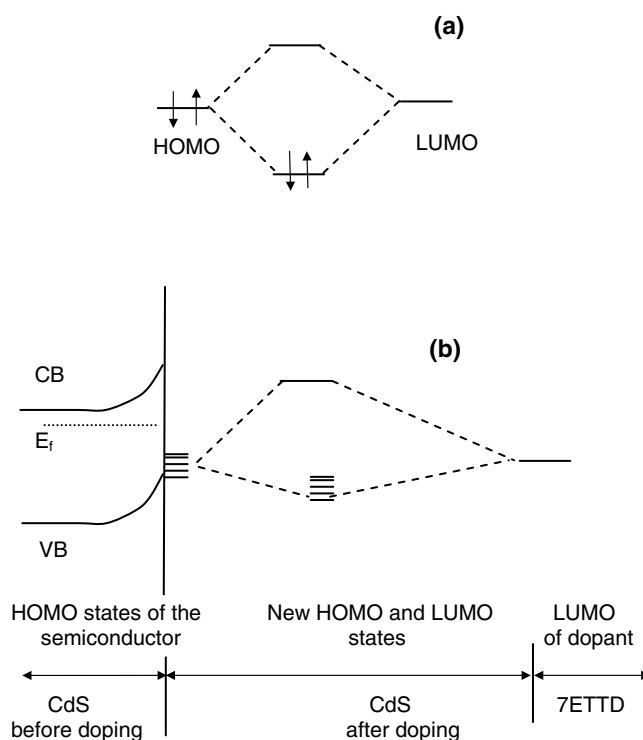


Fig. 5. (a) Conventional MO Diagram of a HOMO–LUMO molecular interaction. (b) MO diagram indicating interaction between surface states of CdS and an adsorbed 7ETTD molecule.

and LUMO levels are participating in creating conduction channels.

The strength of the coupling between molecular orbitals and surface states depends on their mutual location. The greater the energy separation of the levels the smaller interaction will be.

3.2. Model barrier parameters calculations

As mentioned in Section 3.1, at low bias and temperature the I - V curve is linear to a very good approximation. However, for higher voltages the dependence becomes exponential. We employed a WKB approximation to calculate the normalized low-bias (from 0 to ~ 0.2 V) conductance for an assumed TRAPSQR barrier (see Fig. 6). The calculated normalized conductance was fitted to the experimental conductance data. As mentioned earlier, the experimental conductance G - V was obtained from experimental I - V data by numerical differentiation. A standard least-squares function, from a commercially available software package (MATLAB), was used to perform the fitting. The WKB approximation assumes the following expression for tunnel current density:

$$j = \frac{2e}{h} \int_{-\infty}^{\infty} \exp\left(-\frac{2}{\hbar} \int_0^d \left\{2m[\varphi(x, V) - E_x]\right\}^{1/2} dx\right) \times [f(E) - f(E - eV)] dE_x,$$

where h is Planck's constant, $\hbar = h/2\pi$, e is the electronic charge, x is the distance into the barrier, d is the total thickness of the barrier, E is the total energy of the tunneling electrons, E_x is the x component of the energy, and $\varphi(x, V)$ describes the barrier potential. The TRAPSQR barrier potential has the form:

$$\varphi(x, V) = \varphi_1 + (\varphi_2 - \varphi_1)x/d - (x/d + s)V, \quad \text{when } x \leq d, \quad \text{and} \\ \varphi(x, V) = \varphi_3 - (x/d + s)V \quad \text{for } d < x \leq s.$$

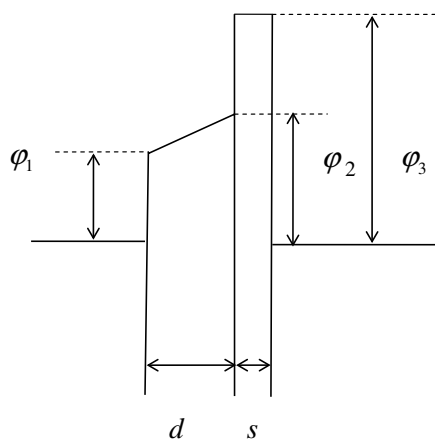


Fig. 6. TRAPSQR barrier used for WKB approximation. φ_1 , φ_2 , and d represent the barrier heights and thickness, respectively, associated with the CdS layer, while φ_3 and s are the barrier height and thickness for an assumed present alumina layer.

φ_1 , φ_2 and d represent the barrier heights and thickness, respectively, associated with the CdS layer (with or without adsorbed 7ETTD), while φ_3 and s are the barrier height and thickness for an assumed present alumina layer. This type of barrier has been used successfully in different types of systems and known to give reasonable results [24,25,18]. Clearly, several possible sets of parameters exist that will satisfy the fit, but only those yielding physically realistic solutions were taken into account. The barrier parameters obtained by fitting the WKB approximation to our experimental G - V data for (i) Al/CdS/Pb and (ii) Al/CdS/7ETTD/Pb junctions, as shown in Figs. 7 and 8, are as follows:

(i) Al/CdS/Pb:

$$\varphi_1 = 3.15 \text{ V}, \quad \varphi_2 = 3.8 \text{ V}, \quad \varphi_3 = 4.59 \text{ V}, \\ d = 0.83 \text{ nm}, \quad s = 0.22 \text{ nm}.$$

(ii) Al/CdS/7ETTD/Pb:

$$\varphi_1 = 2.65 \text{ V}, \quad \varphi_2 = 2.65 \text{ V}, \quad \varphi_3 = 4.60 \text{ V}, \\ d = 2.1 \text{ nm}, \quad s = 0.42 \text{ nm}.$$

The value obtained for φ_3 (~ 4.6 V) is approximately the same for both types of junction, and is due to the presence of small quantities of native Al-oxide. The barrier parameters above seem reasonable, taking into account that the effective barrier parameters in the WKB approximation are average values since the actual area, coverage, and thickness can vary locally. We notice that d increases by 1.27 nm, when 7ETTD is introduced. The calculated length of the 7ETTD molecule is about 0.6 nm (as determined by Gaussian 98 B3LYP/6-31+g(d,2p) calculations) [22] so, on first inspection, it would appear that we have more than one monolayer of 7ETTD adsorbed on the CdS film. However, it must be emphasized that the increase in thickness for the *actual* composite tunnel barrier will include contributions due to (1) the presence of surface hydroxyl groups on the CdS film (see Section 3.3), and (2) any thickening of the native alumina layer. Both of these are possible when the sample is removed from the vacuum chamber, exposed to ambient conditions, and doped with a solution of 7ETTD. We have allowed for thickening of the alumina layer in our calculations, but the contribution due to surface hydroxyl groups has been neglected. This means that the nominal value of 1.27 nm, obtained for the increase in d , is an upper bound and, therefore, consistent with the presence of approximately one adsorbed monolayer of 7ETTD.

The WKB fits for low bias (0 to ~ 0.2 V) are very good and the results above indicate that the dopant decreases the effective barrier height while increasing its thickness. However, WKB fits for voltages above ~ 0.2 V yield poor fits indicating that mechanisms other than tunneling come into play at higher bias. This is also probably why vibrational modes are attenuated in the IET spectra at higher

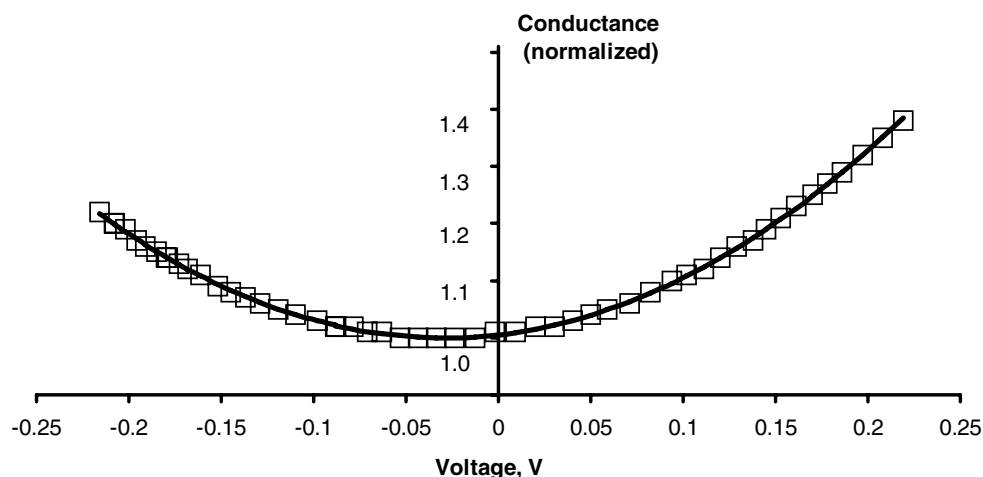


Fig. 7. Normalized conductance–voltage dependence recorded at 4.2 K for an Al/CdS/solvent/Pb tunnel junction (symbols), and WKB approximation fit to the data (solid line).

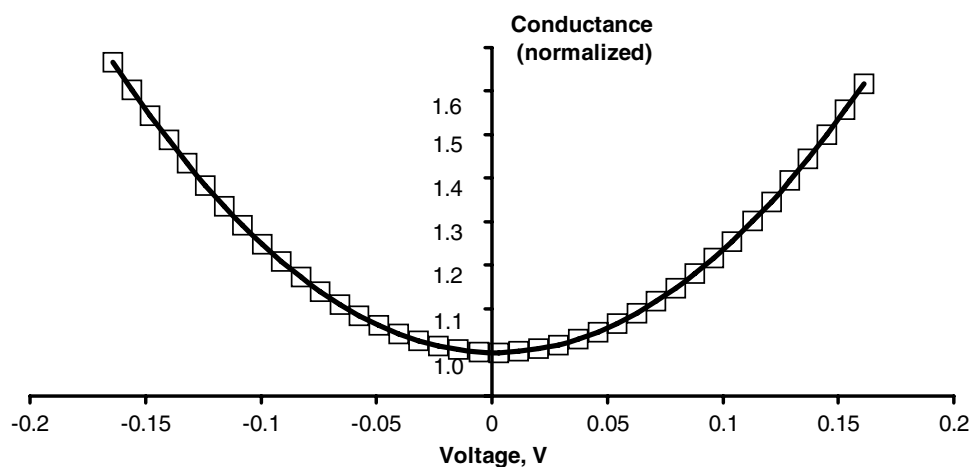


Fig. 8. Normalized conductance–voltage dependence recorded at 4.2 K for an Al/CdS/7ETTD/Pb tunnel junction (symbols), and WKB approximation fit to the data (solid line).

bias since tunneling no longer accounts for the majority of the charge transport through the junctions at this higher bias. Since the HOMO LUMO gap for 7ETTD is too large to decrease the potential barrier, we propose that surface states-orbital coupling occurs, leading to a significantly increased conductance. One also notices that the $G(V, T)$ plot for Al/CdS/Pb is highly asymmetrical because of the barrier height asymmetry (3.15 V and 3.8 V for ϕ_1 and ϕ_2 , respectively). When the molecule is adsorbed on the surface and conducting channels are formed, the barrier becomes more symmetrical, and the corresponding $G(V, T)$ plot is also more symmetrical, since electrons can travel through those channels avoiding tunneling.

3.3. IET, IR, and calculated spectra

Fig. 9 shows control IET spectra obtained from (a) Al/CdS/Pb, (b) Al/CdS/solvent/Pb, and (c) Al/alumina/solvent/Pb junctions which display no evidence of significant contamination. The control spectrum (a) is presented to

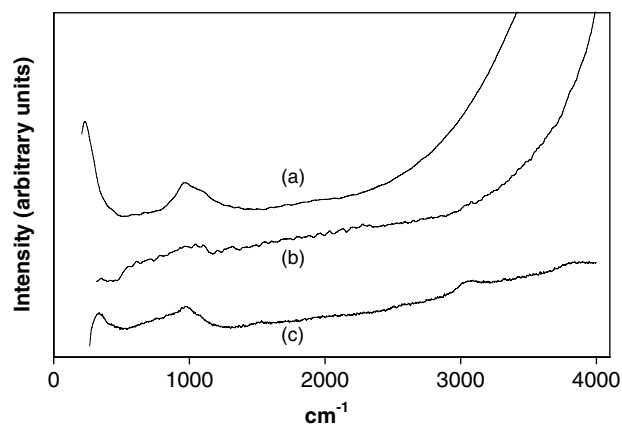


Fig. 9. Control IET spectra obtained from (a) Al/CdS/Pb, (b) Al/CdS/solvent/Pb, and (c) Al/alumina/solvent/Pb junctions.

illustrate peaks normally seen for CdS samples and there is some evidence of Al–O in the spectrum at 980 cm^{-1} . Peaks due to CdS appear as a shoulder at 1110 cm^{-1} and a

smaller feature at 236 cm^{-1} but these peaks cannot be assigned with confidence to particular CdS modes. Spectrum (b) has a broad peak approximately 1100 cm^{-1} due to CdS, and another broad peak approximately 720 cm^{-1} due to bending of surface hydroxyl modes. It has no other discernable features. This spectrum indicates that the solvent neither reacts nor adsorbs on the CdS surface. The peaks present in spectrum (c) are: an Al metal phonon at 300 cm^{-1} , Al–O phonon vibrations approximately 980 cm^{-1} , a broad peak at 3730 cm^{-1} due to stretching of Al–OH, and C–H stretching modes approximately $\sim 3100\text{ cm}^{-1}$. Fig. 10 is a typical IET spectrum obtained from an Al/CdS/7ETTD/Pb sample. (For comparison to conductance–voltage data, note that $1\text{ cm}^{-1} \equiv 8.065\text{ mV}$, so that the spectral range $0\text{--}4000\text{ cm}^{-1}$ corresponds almost exactly to the bias range $0\text{--}500\text{ mV}$. This conversion does not account for the $\sim 8\text{ cm}^{-1}$ superconducting energy gap of the Pb electrode). The downward trend of the background above $\sim 0.2\text{ V}$ ($\sim 1600\text{ cm}^{-1}$) is indirect evidence that tunneling is not a predominant mechanism for conduction at high bias. Usually, similar kinds of backgrounds are observed when Fowler–Nordheim behavior is observed, but as discussed above, the barrier is too high for this and the current voltage characteristics indicate that this mechanism is absent. In order to see spectral lines more clearly we subtracted a fourth-order polynomial fit from the spectrum of Fig. 10 and the resulting spectrum is presented in Fig. 11 together with the corresponding MRAIR spectrum. Table 1

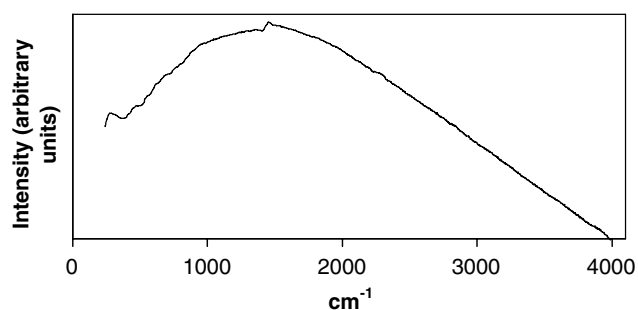


Fig. 10. Typical IET spectrum obtained from an Al/CdS/7-ETTD/Pb junction.

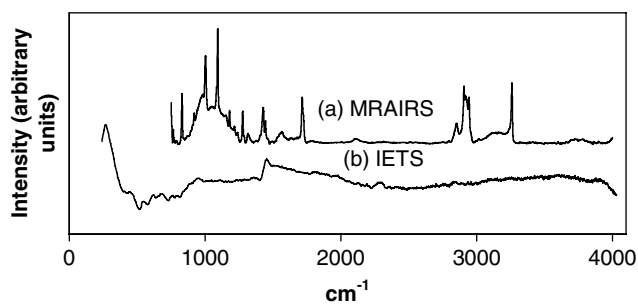


Fig. 11. (a) MRAIR spectrum of CdS layer doped with 7ETTD, (b) IET spectrum obtained of the Al/CdS/7-ETTD/Pb sample of Fig. 10 after subtraction of fourth-order polynomial background.

shows a comparison of MRAIR spectral data for 7ETTD adsorbed on CdS and IR data for a 7ETTD bulk crystalline powder sample. All base peaks match to a large degree. Assignments of the peaks were made based on Gaussian calculations (Gaussian 98 B3LYP/6-31+g(d,2p)) [22] of the vibrational spectrum of the molecule. We now turn to the orientation of 7ETTD on the CdS surface. Based on the MRAIR spectrum, we infer that 7ETTD molecules are adsorbed on CdS via their sulfur crowns. Evidence for this is the $\equiv\text{C-H}$ stretching mode at 3259 cm^{-1} which is very intense indicating that the molecules are oriented such that their triple bonds are aligned essentially perpendicular to the CdS surface, consistent with MRAIRS selection rules. The $\equiv\text{C-H}$ peak is not shifted from its normal bulk value and so the $\equiv\text{C-H}$ group is not expected to interact with the CdS surface. This would be most unlikely in any case since there is no known mechanism for it to do so. Rather, we can be reasonably confident that the sulfur crown at the other end of the molecule bonds to the surface. These observations are in keeping with what one would expect since these compounds have been shown to adsorb via their sulfur crowns on gold [7] and are expected to do the same for other materials. We should mention that identifying direct evidence for vibrational modes associated with the bonding between sulfur atoms in the crown and the CdS surface is difficult with IR spectroscopy because (1) the CdS is amorphous, so there will be a range of expected bond energies, and also (2) they occur at the low end of the IR spectrum where detector sensitivity is very low. However, the MRAIR spectra presented here clearly display strong peaks due to the adsorbed 7ETTD molecules which are in agreement with the model for adsorption via their tri-thia-adamantine anchors discussed above.

We know of no other work to investigate the adsorption of sulfur containing compounds on amorphous CdS. XPS

Table 1
Peak assignments for 7ETTD adsorbed on CdS and for a bulk 7ETTD crystal powder sample

Peak position (cm^{-1})		Assignment
CdS	Bulk	
830	829	Sym breathing mode
920	918	Asym stretch C–C–C (crown), plus CH_2 rocking
1004	1003	Central C–C stretching (top), CH_2 twisting
1083	1084	Asym C–C stretching (crown), CH_2 twisting
1097	1093	Asym C–C stretching (crown), CH_2 twisting
1181	1180	CH (+CH from CH_2) out-of-plane wagging
1218	1219	CH in-plane wagging
1236	1238	CH out-of-plane wagging
1277	1276	CH_2 twisting
1319	1319	CH_2 wagging
1429	1427	CH_2 scissoring
1445	1446	(all) CH_2 scissoring
1715	–	C=O (contamination)
2104	2100	C \equiv C stretching
2907	2907	Sym C–H (CH_2) stretching
2945	2945	Sym C–H (CH_2) stretching
3259	3259	$\equiv\text{C-H}$ stretching

is a technique that one might consider to investigate this further, but the ability of XPS to detect any sulfur peaks related to molecule-CdS surface interactions is extremely doubtful because a surface-related sulfur peak would be expected to appear as a shoulder on the essentially bulk background sulfur peak from the CdS layer and with an intensity several orders of magnitude weaker. MRAIRS appears to be a far better way to investigate the adsorption mechanisms.

4. Conclusions

IET and MRAIR spectroscopic data indicate that 7ETTD molecules self-assemble and adsorb on ultra-thin CdS films via their adamantane anchors such that they are aligned with their axes essentially perpendicular to the surface. The MRAIRS data, in particular, are more conclusive than IETS and strongly suggest that the molecules are adsorbed via their trithia-adamantane anchors. The adsorbed 7ETTD layer significantly modifies the conductance–voltage behavior of the tunnel junctions under investigation and it is observed that tunneling is no longer the predominant conduction mechanism for junction biases above ~ 0.2 V. At these higher biases a frontier orbital coupling mechanism between HOMO and LUMO levels of the 7ETTD molecules and surface states on the CdS offers a plausible explanation for the observed conductance–voltage behavior. Due to the significant effect on junction behavior it appears that further investigation of this family of compounds, with particular attention to their applicability in molecular electronics, is justified.

References

- [1] A. Aviram, M.A. Ratner, *Chem. Phys. Lett.* 29 (1974) 277.
- [2] D.L. Allara, R.G. Nuzzo, *Langmuir* 1 (1985) 45.
- [3] N.E. Schlotter, M.D. Porter, T.B. Bright, D.L. Allara, *Chem. Phys. Lett.* 132 (1986) 93.
- [4] D.Y. Huang, Y.-T. Tao, *Bull. Inst. Chem. Acad. Sin.* 33 (1986) 73.
- [5] S. Devdas, R.R. Mallik, *Int. J. Adhes. Adhes.* 20 (2000) 355.
- [6] G.E. Poirier, *J. Vac. Sci. Technol. B* 14 (1995) 1453.
- [7] Jun Hu, Yubiao Liu, Chalermchai Khemtong, Jouliana M. El Khoury, Timothy J. McAfoos, Ian S. Taschner, *Langmuir* 20 (2004) 4933.
- [8] Jun Hu, US patent numbers WO 2005003089 A2, and WO 2005003089 A3, 2005.
- [9] S. Guha, R.A. Haight, N.A. Bojarczuk, D.W. Kisker, *J. Appl. Phys.* 82 (1997) 4126.
- [10] M. Ozaki, D. Peebles, B.R. Weinberger, A.J. Heeger, A.G. MacDiarmid, *J. Appl. Phys.* 51 (8) (1980) 4252.
- [11] R.R. Mallik, T. Butler Jr., W.J. Kulnis Jr., B. DeVier, *J. Appl. Phys.* 73 (1993) 2347.
- [12] R.C. Jaklevic, J. Lambe, *Phys. Rev. Lett.* 17 (1966) 1139.
- [13] P.K. Hansma (Ed.), *Tunneling Spectroscopy, Capabilities, Applications, and New Techniques*, Plenum, New York, 1982.
- [14] N.M.D. Brown, in: R.J.H. Clark, R.E. Hester (Eds.), *Spectroscopy of Surfaces*, John Wiley and Sons, New York, 1988 (Chapter 5).
- [15] K.W. Hipps, U. Mazur, in: J.M. Chalmers, P.R. Griffiths (Eds.), *Handbook of Vibrational Spectroscopy*, John Wiley and Sons, New York, 2002, p. 812.
- [16] R.R. Mallik, S. Anabtawi, B. Moore, T.A. Hartman, *Surf. Sci.* 380 (1997) 124.
- [17] R.R. Mallik, P.N. Henriksen, T. Butler Jr., W.J. Kulnis Jr., *T. Confer, J. Vac. Sci. Technol. A* 10 (1992) 2412.
- [18] I. Dolog, R.R. Mallik, D. Malz, A. Mozynski, *J. Appl. Phys.* 95 (2004) 3075.
- [19] Y. Wang, R.R. Mallik, P.N. Henriksen, *Rev. Sci. Instrum.* 64 (1993) 890.
- [20] T.R. Seman, R.R. Mallik, *Rev. Sci. Instrum.* 70 (1999) 2808.
- [21] S. Devdas, R.R. Mallik, R. Coast, P.N. Henriksen, *Surf. Sci.* 326 (1995) 327.
- [22] M.J. Frisch, G.W. Trucks, H.B. Schlegel, G.E. Scuseria, M.A. Robb, J.R. Cheeseman, V.G. Zakrzewski, J.A. Montgomery Jr., R.E. Stratmann, J.C. Burant, S. Dapprich, J.M. Millam, A.D. Daniels, K.N. Kudin, M.C. Strain, O. Farkas, J. Tomasi, V. Barone, M. Cossi, R. Cammi, B. Mennucci, C. Pomelli, C. Adamo, S. Clifford, J. Ochterski, G.A. Petersson, P.Y. Ayala, Q. Cui, K. Morokuma, D.K. Malick, A.D. Rabuck, K. Raghavachari, J.B. Foresman, J. Cioslowski, J.V. Ortiz, A.G. Baboul, B.B. Stefanov, G. Liu, A. Liashenko, P. Piskorz, I. Komaromi, R. Gomperts, R.L. Martin, D.J. Fox, T. Keith, M.A. Al-Laham, C.Y. Peng, A. Nanayakkara, M. Challacombe, P.M.W. Gill, B. Johnson, W. Chen, M.W. Wong, J.L. Andres, C. Gonzalez, M. Head-Gordon, E.S. Replogle, J.A. Pople, Gaussian, Inc. Pittsburgh PA, 1998.
- [23] R. Cohen, L. Kronik, A. Vilan, A. Shanzer, D. Cahen, *Adv. Mater.* 12 (2000) 33.
- [24] D.G. Walmsley, R.B. Floyd, W.E. Timms, *Solid State Commun.* 22 (1977) 497.
- [25] L.D. Bell, R.V. Coleman, *Phys. Rev. B* 30 (1984) 4120.